Pressure-Induced Collapse of Magnetic Order in Jarosite

Ryan A. Klein,[1] James P. S. Walsh,[1] Samantha M. Clarke,[2] Zhenxian Liu,[3] E. Ercan Alp,[4] Wenli Bi,[5] Yue Meng,[6] Alison B. Altman,[1] Paul Chow,[6] Yuming Xiao,[6] M. R. Norman,[7,*] James M. Rondinelli,[8,*] Steven D. Jacobsen,[9,*] Danilo Puggioni,[8,*] and Danna E. Freedman[1,*]

[1]*Department of Chemistry, Northwestern University, Evanston, Illinois 60208, USA*
[2]*Lawrence Livermore National Laboratory, 7000 East Ave, Livermore, California 94550, USA*
[3]*Department of Physics, University of Illinois at Chicago, Chicago, Illinois 60607, USA*
[4]*Advanced Photon Source, Argonne National Laboratory, 9700 South Cass Avenue, Lemont, Illinois 60439, USA*
[5]*Department of Physics, University of Alabama at Birmingham, Birmingham, Alabama 35294, USA*
[6]*HPCAT, X-Ray Science Division, Argonne National Laboratory, Lemont, Illinois 60439, USA*
[7]*Materials Science Division, Argonne National Laboratory, Argonne, Illinois 60439, USA*
[8]*Department of Materials Science and Engineering, Northwestern University, Evanston, Illinois 60208, USA*
[9]*Department of Earth and Planetary Sciences, Northwestern University, Evanston, Illinois 60208, USA*

(Received 7 April 2020; accepted 21 July 2020; published 13 August 2020; corrected 13 October 2020)

We report a pressure-induced phase transition in the frustrated kagomé material jarosite at ~45 GPa, which leads to the disappearance of magnetic order. Using a suite of experimental techniques, we characterize the structural, electronic, and magnetic changes in jarosite through this phase transition. Synchrotron powder x-ray diffraction and Fourier transform infrared spectroscopy experiments, analyzed in aggregate with the results from density functional theory calculations, indicate that the material changes from a $R\bar{3}m$ structure to a structure with a $R\bar{3}c$ space group. The resulting phase features a rare twisted kagomé lattice in which the integrity of the equilateral Fe^{3+} triangles persists. Based on symmetry arguments we hypothesize that the resulting structural changes alter the magnetic interactions to favor a possible quantum paramagnetic phase at high pressure.

DOI: 10.1103/PhysRevLett.125.077202

Spins arrayed on lattices exhibiting magnetic frustration can engender exotic magnetic phases [1–4]. Materials that host these lattices have been intensely researched for several decades, including the antiferromagnetic mineral jarosite, $KFe_3(OH)_6(SO_4)_2$ [5–15]. Jarosite's kagomé lattice—in which high-spin Fe^{3+} ions ($S = 5/2$) form a corner-shared triangular lattice—frustrates magnetic ordering. The Néel temperature, T_N, of jarosite at ambient pressure is 65 K—much lower than may be expected given the Curie-Weiss temperature of −828 K, leading to a frustration parameter of $f = 12.7$, where $f \geq 10$ is considered frustrated [9,16,17].

The ordered magnetic structure of jarosite arises from two primary interactions [10–14]. The first is a nearest neighbor antiferromagnetic superexchange interaction along the Fe-O-Fe pathway within the kagomé lattice. The second is an antisymmetric Dzyaloshinskii-Moriya (DM) interaction [18,19]. The DM vectors, **D**, are confined within the mirror plane bisecting the Fe^{3+} ions [12,18–21]. These interactions select the $q = 0$ spin structure which features a magnetic umbrella motif with a uniform positive vector chirality and a small canting of the spins out of the plane [12–14]. This canting alternates from plane to plane, but an applied magnetic field can align them leading to a net ferromagnetic moment [12].

Extensive theoretical work hints at a rich phase diagram for frustrated kagomé antiferromagnets in the presence of a DM interaction [12,22–30]. These studies predict quantum critical points between the $q = 0$ state and other magnetic phases that are potentially accessible in jarosite by manipulating the exchange interactions. To that end, high applied pressures offer a vector to tune the phase stability [31–35], structure, and magnetism in frustrated materials analogous to variable magnetic fields and chemical composition. High applied pressures shorten interatomic distances, which impact the potential energy landscapes and magnetic exchange pathways for the realization of exotic phases of matter [36–41]. Moreover, applied pressure also offers a route to access magnetically frustrated variants of parent lattices that may be difficult to access synthetically at ambient conditions, which may also host exotic magnetic phases. Despite the growing body of experimental work in this area, complete PT phase diagrams for kagomé lattice materials—and other frustrated lattices featuring competing exchange and DM interactions—remain absent.

Here, we report the high-pressure quenching of magnetic order in jarosite leading to a possible quantum paramagnetic phase. We study the crystal, electronic, and magnetic structure of jarosite at pressures up to 121 GPa using a suite of *in situ* diamond anvil cell (DAC) techniques [42].

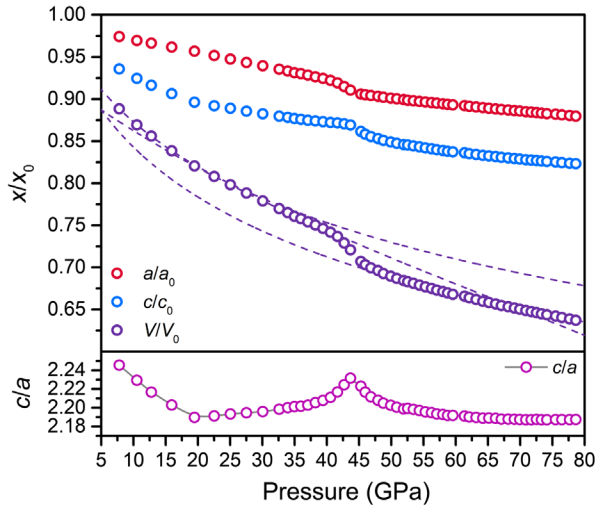

FIG. 1. The normalized lattice parameters for jarosite at ambient temperature are plotted as a function of pressure (top). These values were obtained from Pawley fits of the PXRD data using the $R\bar{3}m$ space group for the jarosite phase. The plot of c/a vs pressure highlights the phase transitions at $P^{*,1}$ and $P^{*,2}$. The spline interpolation in the plot of c/a vs pressure, which lies behind the data points over the entire measure pressure range, is a guide for the eye. Unless shown, error bars are commensurate with the symbol size. The dashed lines in the figure (top) are the normalized equation of state curves for the volume data (see Table S3 for parameters and Figs. S3–S6 in the Supplemental Material [46].).

We identify a symmorphic-to-nonsymmorphic transition from $R\bar{3}m$ to $R\bar{3}c$. The calculated $R\bar{3}c$ structure exhibits equilateral triangles of Fe^{3+} ions that twist, but do not distort, to yield a rare twisted kagomé lattice with a unit cell that doubles along the c axis. This conclusion is supported by a Rietveld refinement analysis of a high-pressure PXRD pattern. The lowering in symmetry is supported by Fourier-transform infrared spectroscopy (FTIR) measurements. Variable-temperature and -pressure synchrotron Mössbauer spectroscopy (SMS) measurements reveal a collapse of detectable magnetic order at pressures above 43.7(4) GPa down to 20 K, which we discuss in the context of the pressure-tuned exchange interactions on the twisted kagomé lattice to conjecture the existence of a quantum paramagnetic phase.

To search for potential pressure-driven phase transitions in jarosite, we collected powder x-ray diffraction (PXRD) patterns up to 78.6 GPa at ambient temperature. We extracted the unit cell lattice parameters at each pressure by applying a Pawley fit to the diffraction patterns (Fig. 1, top) [43–45]. Pawley fits using the ambient-pressure $R\bar{3}m$ structure model the data well across the entire measured pressure range. Up to 19.5(1) GPa, an initial third-order Birch Murnaghan equation-of-state (BM3) curve accurately models the data (Table S3 [46]) [71,72]. There is an isosymmetric transition at $P^{*,1} = 19.5(1)$ GPa, discernable from the inflection point in the c/a ratio at this pressure (Fig. 1, bottom). Between 19.5 and 39.4 GPa, a second BM3 equation of state curve accurately models the data. We find a transition at $P^{*,2} = 43.7(4)$ GPa where an unusual cusp in c/a occurs, signaling a complicated structural transition at this pressure. From 49.9 to 78.6 GPa, the data are well modelled with a third BM3 equation of state curve.

To better understand this complex behavior under compression, we conducted DFT calculations to search for possible pressure-induced lattice instabilities. We constrained the volume of the unit cell to the observed volume at a given pressure and calculated the phonon modes every ten GPa up to 80 GPa. We find a soft phonon at the T (0,0, 3/2) point of the Brillouin zone between 30 and 40 GPa (Fig. S31 [46]). Upon condensing the instability followed by atomic relaxation, we find a new high-pressure structure ($R\bar{3}c$ space group) that emerges from the known ambient pressure $R\bar{3}m$ structure. The two space groups have a group-subgroup relationship such that the transition is driven by a T_2^+ mode, which doubles the length of the c axis due to the glide operation. The new, high-pressure $R\bar{3}c$ structure is characterized by a twisted kagomé lattice in which uniform Fe-Fe contacts form equilateral triangles that twist slightly relative to the parent kagomé lattice. At the same time, both apical oxygen ions shift in the same direction, enhancing the distortion of the FeO_6 octahedra. We distinguish this lattice from the highly distorted triangular-kagomé lattice [73], in which next near neighbor magnetic ions are connected by direct superexchange pathways. We analyzed the PXRD patterns over the entire measured pressure range considering both the $R\bar{3}m$ and $R\bar{3}c$ structures. We found that the Pawley fits of the patterns above the phase transition using the calculated $R\bar{3}c$ structure give comparable fit statistics to the Pawley fits which used the $R\bar{3}m$ structure. Additionally, the normalized lattice parameters qualitatively agree well with those obtained from the previous Pawley fits (Figs. S7–S10 [46]).

To investigate the possible lowering in symmetry at $P^{*,2}$, we conducted ambient temperature FTIR measurements in the mid-IR (500–6000 cm^{-1}) up to 54.4 GPa (Figs. S12–S21) [46,74–76]. At 45.5(4) GPa, there is a first order discontinuity in the IR modes. We observe an increase in the number of observed modes in the measured region in agreement with the calculated lowering in symmetry at the $R\bar{3}m$ to $R\bar{3}c$ transition. The calculated number of IR active modes exceeds the observed number of modes at all measured pressures and there is good qualitative agreement for the pressure-dependent dispersion between the calculated and the observed modes (Figs. S20 and S21 [46]). These data support the DFT predicted symmorphic-to-nonsymmorphic transition.

To test the validity of the calculated structures at $P > P^{*,2}$, we performed a Rietveld refinement analysis of a selected representative PXRD pattern collected at 62.1(6) GPa. The details of the Rietveld refinement and

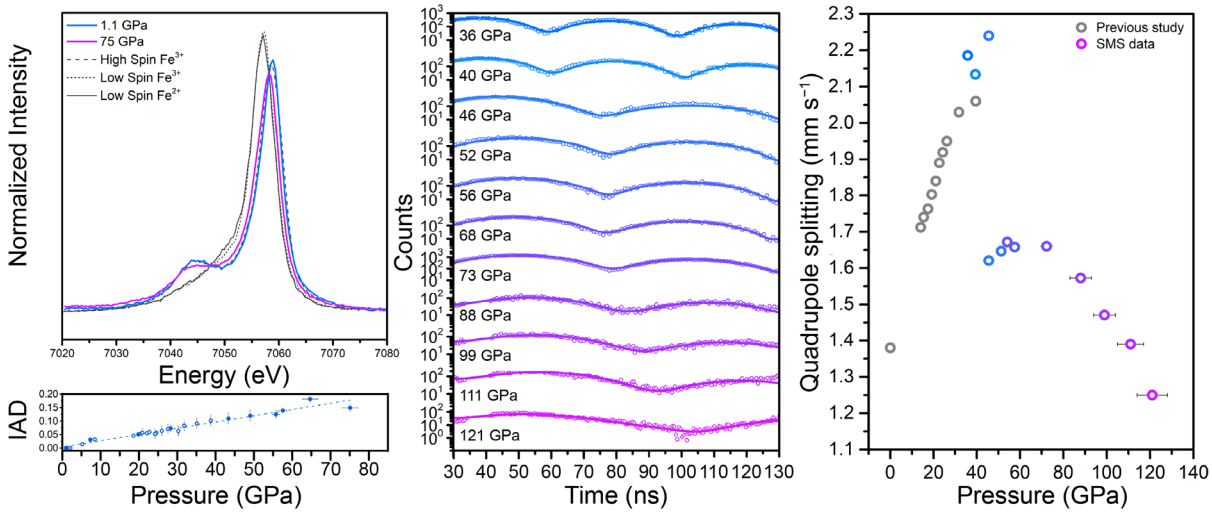

FIG. 2. The normalized XES data (left) illustrate that the electronic structure changes linearly with pressure, as shown by the plot of the IAD value vs pressure in the inset of the XES plot. The data from jarosite measured at 1.1 GPa overlays the high-spin Fe^{3+} reference data. In the plot of the IAD values, closed symbols originate from spectra reported herein, whereas open symbols originate from previously reported spectra [42]. The SMS data (center) show a change in spectral shape between 39.5 and 45.6 GPa. Spurious signals in the SMS data above 80 GPa are masked between 36 and 41 ns. Open circles denote the data points while the solid lines show the fits to these data. Fits of the data reveal a first order discontinuity in ΔE_Q (right), which decreases from 2.24(2) to 1.62(2) mm s^{-1} through the phase transition at 43.7(4) GPa. Unless shown, error bars are commensurate with the symbol size. Open gray circles are previously reported data for the ΔE_Q plot [42]. See Fig. S23 in the Supplemental Material [46] for an enlarged plot of the IAD values as a function of pressure.

structure solution are given in the Supplemental Material [46] (S9–S11), and the results are summarized in Table S7. The Rietveld refinement using the $R\bar{3}c$ structure fits the experimental PXRD pattern well (fit statistics are listed in Table S7 [46]). In addition, the $R\bar{3}c$ structure is internally consistent with the FTIR measurements, while the other structures suggested by the DFT calculations are not. Therefore, based on the Rietveld refinement fits—analyzed in conjunction with the FTIR results and DFT calculations—we conclude that the high-pressure phase of jarosite is accurately described by the $R\bar{3}c$ structure and possesses a twisted kagomé lattice.

To probe the local electronic structure of the Fe ions in the high-pressure phase ($P > P^{*,2}$), we conducted nonresonant x-ray emission spectroscopy (XES) measurements as well as ambient-temperature, variable-pressure SMS measurements on pure single crystals of jarosite. Figure 2 (left) summarizes the XES experiments. Up to 75 GPa, the $K\beta_{1,3}$ line redshifts slightly and decreases in intensity. The $K\beta'$ feature decreases in intensity slightly across this same pressure interval but does not shift in energy. We quantified the extent of the spectral changes as a function of pressure, using the integral of the absolute value of the difference of the curves method (IAD) [77] (Fig. 2, left, inset). The IAD values follow a linear trend with pressure ($R^2 = 0.9556$). The absence of discontinuities in the plot of the IAD values vs pressure confirms that there are no phase transitions in the local electronic structure of the Fe^{3+} ions. Based on these findings, we conclude that the spin state of the Fe^{3+} ions ($S = 5/2$) remains constant up to 75 GPa [78–80]. We attribute the observed spectral changes to an increase in the covalent nature of the Fe-O bonds in the distorted FeO_6 octahedra in the kagomé planes [78,79,81]. Additionally, we reference our data in Fig. 2 with previously published data for compounds with established valence and spin states, including hematite, Fe_2O_3 (high-spin Fe^{3+}), measured at ambient conditions and phase D, $MgSi_{1.5}Fe_{0.15}Al_{0.32}H_{2.6}O_6$ (low-spin Fe^{3+}), measured at 93 GPa and ambient temperature [78], to show that no spin-state transition occurs up to 75 GPa. We also use reported data for $Mg_{0.75}Fe_{0.25}O$ measured at 90 GPa as a low-spin Fe^{2+} reference [82].

We further probed the local electronic and structural environment around the Fe^{3+} ions using SMS experiments [83–88] at ambient temperature up to 121 GPa (Fig. 2, center). This technique is analogous to ambient pressure, offline Mössbauer experiments, and as such, yields the quadrupole splitting and magnetic hyperfine terms at elevated pressures. We fit these data to extract the quadrupole splitting values (ΔE_Q; Fig. 2, right) [89]. ΔE_Q increases linearly with pressure from ~1.4 mm s^{-1} at ambient pressure to 2.13(2) mm s^{-1} at 39.5 GPa [42]. The spectrum at 45.6 GPa was fit with two phases, one with $\Delta E_Q = 2.24(2)$ mm s^{-1} and one with $\Delta E_Q = 1.62(2)$ mm s^{-1}. At this pressure, there is a first order discontinuity in ΔE_Q. Above the pressure-induced discontinuity, ΔE_Q remains relatively constant between 1.6

and 1.7 mm s^{-1} up to 72.3 GPa and then decreases monotonically with additional pressure [90,91].

The magnitude of ΔE_Q stems from the asymmetry of the electric field gradient around the Mössbauer active ion [92,93]. In general, ΔE_Q is influenced by two factors: the symmetry of the electronically populated orbitals and the lattice contribution. In jarosite (d^5, high spin, nominal ^6S ground state), the nonzero value of ΔE_Q comes from the FeO_6 tetragonal elongation and from the differences in the σ- and π-donor ability between the equatorial μ_2-OH ligands compared to the axial sulfate ligands. One explanation for this behavior would be a spin crossover transition, however, within the resolution of the XES experiments, the IAD analysis shows no discontinuities in the electronic structure of the Fe^{3+} ions up to 75 GPa. The combination of these data suggests the discontinuity in the ΔE_Q vs pressure relationship arises from the sudden change in the lattice contribution to the asymmetry of the electric field gradient. The first order discontinuity in the plot of ΔE_Q vs pressure therefore supports the calculated structural transition from the $R\bar{3}m$ to the $R\bar{3}c$ phase.

We probed the magnetic ordering temperature in jarosite by fitting the SMS data and extracting the magnetic hyperfine term, B_{HF}. B_{HF} is the magnitude of Zeeman splitting of the m_I sublevels probed in Mössbauer spectroscopy [92,93]. Here, a nonzero B_{HF} arises from magnetic ordering. A nonzero B_{HF} term creates readily apparent additional quantum beats in the SMS spectra that occur with greater frequency, and the lack of the onset of magnetic ordering as a function of pressure in the data presented in Fig. 2 is clear from the lack of additional quantum beats [42,83–88,92,93]. Further details concerning the fitting of the data to extract the relevant Mössbauer terms can be found in the Supplemental Material [46]. From these data, we extend the temperature-pressure magnetic phase diagram for jarosite to above 100 GPa in pressure (Fig. 3). T_N for jarosite increases linearly with pressure up to ~40 GPa. This trend can be explained by considering the pressure-induced change in the equatorial Fe-O bond distances,$d(\mathrm{Fe}-\mathrm{O})_{\mathrm{eq}}$. This bond distance decreases with increasing pressure [42]. This affects both the exchange interactions J and $\mathbf{D}$ as the Fe-3d to O-2p hopping integral t_{pd} typically scales as $d(\mathrm{Fe}-\mathrm{O})_{\mathrm{eq}}^{-4}$. These interactions combine to yield a linear increase in T_N up to ~40 GPa. Then, the variable-temperature, isobaric dataset measured at ~47 GPa—just above $P^{*,2}$—exhibits a B_{HF} value of zero for all measured temperatures down to the lowest measured temperature of 29.3 K. The disappearance of the B_{HF} term indicates a collapse of the magnetic order coincident in pressure with the structural phase transition observed in the PXRD [43.7(4) GPa] and FTIR [45.5(4) GPa], predicted by the DFT calculations (~40 GPa), and inferred from the aggregate of the XES data and the ΔE_Q vales from the SMS experiments [45.6(4) GPa].

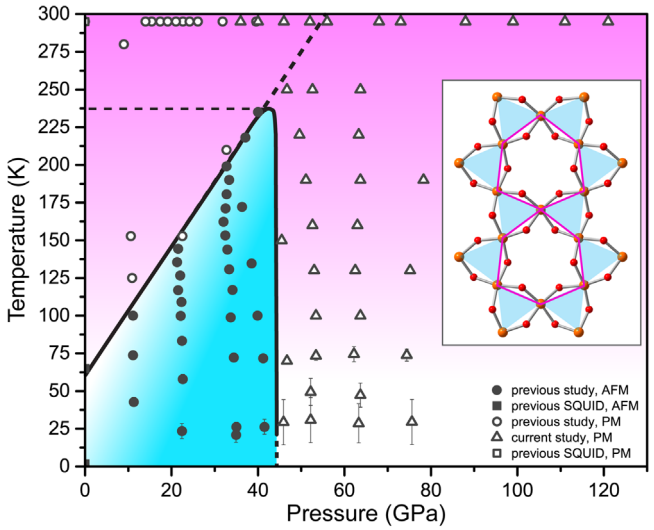

FIG. 3. The temperature-pressure magnetic phase diagram for jarosite up to 121 GPa. Closed symbols denote antiferromagnetic order. Open symbols denote measurements in which no magnetic ordering is observed. The antiferromagnetic region is highlighted in blue while the paramagnetic region is highlighted in pink. In the legend, AFM denotes antiferromagnetic ordering, while PM denotes paramagnetic. The measured values from a previous study are reported in Ref. [42]. The dashed lines indicate the linear trajectory of T_N with pressure and the maximum measured T_N value. In the inset, blue equilateral triangles and distorted pink hexagons highlight the twisted kagomé lattice of Fe^{3+} ions at 80 GPa in the $R\bar{3}c$ phase. Iron and oxygen ions are depicted as orange and red spheres, respectively, while the other atoms are omitted for clarity.

The observed magnetic collapse indicates either the addition or loss of an exchange interaction, and/or a drastic change in the existing exchange interactions. At ambient pressure, there are two principal symmetric exchange couplings, J_1 (near neighbor) and J_2 (next near neighbor), and two components of the antisymmetric exchange interaction $\mathbf{D}_{\mathrm{ij}}$, the out-of-plane $\mathbf{D}_z$ and the in-plane $\mathbf{D}_\rho$ (i and j are site indices). An analysis of the spin wave dispersions (in Ref. [17]) at ambient pressure shows that (in meV) $J_1 = 3.18$, $J_2 = 0.11$, $|\mathbf{D}_\rho| = 0.197$, and $\mathbf{D}_z = -0.196$. J_1 is determined by the Fe-O-Fe pathway. J_2 is determined by an Fe-O-O-Fe super-super-exchange pathway, which explains why it is relatively weak compared to J_1. $\mathbf{D}$ is constrained to lie within the mirror plane bisecting the two iron atoms and thus normal to the Fe-Fe contact that comprises the equilateral triangles of the lattice [19,20].

The transition from the $R\bar{3}m$ phase to the $R\bar{3}c$ structure modifies the interatomic distances and angles and therefore affects these exchange interactions (Fig. 3, inset). The bond angle in the Fe-O-Fe pathway does not change drastically with pressure through the phase transition (Fig. S32 in the Supplemental Material [46]). However, the planar O ion moves off center between the two Fe^{3+} ions, creating inequivalent bond distances $d(\mathrm{Fe}-\mathrm{O})_1$ and $d(\mathrm{Fe}-\mathrm{O})_2$.

Despite this, the equilateral triangles of Fe^{3+} ions remain intact as each Fe^{3+} ion has two $d(Fe-O)_1$ and two $d(Fe-O)_2$ distances. Thus, we do not expect J_1 to change drastically across $P^{*,2}$. Conversely, the super-super-exchange J_2 splits into J_{2a} and J_{2b}. However, the changes in bond lengths and angles are such that we expect both to remain small compared to J_1. As with the ambient pressure phase, we expect that the interplane couplings remain negligible in the $R\bar{3}c$ structure.

The loss of the mirror plane between the Fe^{3+} ions removes a symmetry constraint for the direction of $\mathbf{D}$ [20] which could influence the magnetic order. In the ambient-pressure $R\bar{3}m$ structure, $\mathbf{D}$ is constrained to lie within the mirror plane, with a negative $\mathbf{D}_z$ stabilizing a positive vector chirality and $\mathbf{D}_\rho$ causing canting of the spins out of the plane [12,17]. When the mirror plane is removed in the $R\bar{3}c$ structure, the symmetry constraint lifts and $\mathbf{D}_\rho$ can rotate, although we anticipate that this rotation is small. Moreover, the positive vector chirality state is still allowed in the $R\bar{3}c$ space group [94].

Instead, we hypothesize that a pressure-driven quenching of the antisymmetric exchange produces the observed vanishing of magnetic order. At ambient pressure, $\mathbf{D}$ lifts the energy of the kagomé zero modes which in turn promotes long-range magnetic order and explains the relatively high T_N [14,17]. In the $R\bar{3}c$ structure, the apical oxygen ions shift and the $(Fe-O)_{eq}$ bond splits lifting any remnant degeneracy in the crystal field splittings. This acts to quench any orbital angular momentum L arising from mixing with low-lying excited states. As $\mathbf{D}$ is proportional to L, a quenching of L at high pressures would quench the DM term and effectively lower the zero modes back towards zero energy. The same arguments apply to the single-ion anisotropy which is an alternate source of zero mode lifting [14,17]. This could be investigated in the future by high temperature susceptibility measurements and Fe L-edge [95] spectroscopy at high pressure to test for a deviation of the Fe ions from the $S=5/2$, $L=0$ state. We note that the material may be magnetically ordered at temperatures below the limit of detection of these experiments, suggesting future investigations into the magnetic structure at these extreme conditions.

Based on the data herein, we exclude certain possible magnetic ground states in the measured region. We exclude as a possibility a spin glass state, which shows signatures in Mössbauer measurements that are not observed herein [96]. Likewise, we exclude a conventional quantum spin liquid state or a valence bond solid state given the classical nature of $S=5/2$ spins [1–4,97,98]. From the vanished B_{HF}, we conclude that the pressure-induced phase is distinct from the field-induced phase in jarosite [12]. Lastly, a nonzero value of the Coulomb repulsion U is required to maintain a high spin state at high pressure in the DFT calculations, and as such the material is predicted to remain insulating across $P^{*,2}$ (Fig. S33 in the Supplemental Material [46]). The results of the DFT calculations imply that an insulator-to-metal Mott transition does not occur. Additionally, we do not observe any optical signatures of metallization with pressure [99,100]. However, the observed linear increase in T_N followed by a dramatic quenching of magnetic order is similar to the pressure-induced metallization events which occur in several transition metal halides [101–103] and we anticipate that future studies of the resistivity of this material at extreme conditions will be extremely illuminating.

Our unexpected finding of the dramatic collapse of the magnetically ordered $q=0$ state in jarosite at high pressure suggests there is much remaining to be discovered in the phase space of 2D magnetically frustrated materials. Additional theoretical and experimental work on the rare twisted kagomé lattice with competing symmetric and antisymmetric exchange interactions will contribute to our understanding of this unusual phenomenon.

We thank Dr. S. N. Tkachev, Dr. D. Zhang, and Dr. C. Kenney-Benson for technical support. We thank Dr. E. C. Thompson for wonderful discussions. Creating and understanding magnetic frustration in synthetically derived materials was supported by the ARO (W911NF1810006). Initial work to develop high pressure methodologies was supported by the AFOSR (FA9550-17-1-0247). S. D. J. acknowledges support from the Capital/DOE Alliance Center (CDAC) for beamtime at HPCAT, the NSF (EAR-1452344), and the David and Lucile Packard Foundation. D. P. and J. M. R. acknowledge the Army Research Office under Grant No. W911NF-15-1-0017 for financial support and the Department of Defense High Performance Computing Modernization Program (DOD-HPCMP) for computational resources. W. B. was partially supported by the Consortium for Materials Properties Research in Earth Sciences (COMPRES). M. R. N. is supported by the Materials Sciences and Engineering Division, Basic Energy Sciences, Office of Science, US DOE. Part of this work was performed under the auspices of the U.S. Department of Energy by Lawrence Livermore National Security, LLC, under Contract No. DE-AC52-07NA27344. The gas loading was also partially supported by COMPRES under the NSF Cooperative Agreement EAR-1634415. HPCAT operations are supported by DOE-NNSA's Office of Experimental Sciences. The National Science Foundation —Earth Sciences (EAR-1634415) and Department of Energy—Geosciences (DE-FG02-94ER14466) support GSECARS. Experiments at Sector 13-BM-C were conducted under the Partnership for Extreme Crystallography (PX^2), which is also supported by COMPRES. The APS is a U.S. Department of Energy (DOE) Office of Science User Facility operated for the DOE Office of Science by ANL under Contract No. DE-AC02-06CH11357.

*Corresponding authors.
danna.freedman@northwestern.edu
norman@anl.gov
jrondinelli@northwestern.edu
s-jacobsen@northwestern.edu
danilo.puggioni@northwestern.edu

[1] P. W. Anderson, Science **235**, 1196 (1987).
[2] C. Broholm, R. J. Cava, S. A. Kivelson, D. G. Nocera, M. R. Norman, and T. Senthil, Science **367**, eaay0668 (2020).
[3] L. Savary and L. Balents, Rep. Prog. Phys. **80**, 016502 (2016).
[4] L. Balents, Nature (London) **464**, 199 (2010).
[5] G. Klingelhöfer, R. V. Morris, B. Bernhardt, C. Schröder, D. S. Rodionov, P. De Souza, A. Yen, R. Gellert, E. Evlanov, B. Zubkov *et al.*, Science **306**, 1740 (2004).
[6] S. M. McLennan, J. F. Bell, III, W. Calvin, P. Christensen, B. C. Clark, P. De Souza, J. Farmer, W. H. Farrand, D. A. Fike, R. Gellert *et al.*, Earth Planet. Sci. Lett. **240**, 95 (2005).
[7] J. M. Bigham, U. Schwertmann, S. J. Traina, R. L. Winland, and M. Wolf, Geochim. Cosmochim. Acta **60**, 2111 (1996).
[8] M. E. E. Madden, R. J. Bodnar, and J. D. Rimstidt, Nature (London) **431**, 821 (2004).
[9] D. G. Nocera, B. M. Bartlett, D. Grohol, D. Papoutsakis, and M. P. Shores, Chem. Eur. J. **10**, 3850 (2004).
[10] D. Grohol and D. G. Nocera, J. Am. Chem. Soc. **124**, 2640 (2002).
[11] D. S. Inosov, Adv. Phys. **67**, 149 (2018).
[12] D. Grohol, K. Matan, J.-H. Cho, S.-H. Lee, J. W. Lynn, D. G. Nocera, and Y. S. Lee, Nat. Mater. **4**, 323 (2005).
[13] D. Grohol, D. G. Nocera, and D. Papoutsakis, Phys. Rev. B **67**, 064401 (2003).
[14] T. Yildirim and A. B. Harris, Phys. Rev. B **73**, 214446 (2006).
[15] T. Inami, M. Nishiyama, S. Maegawa, and Y. Oka, Phys. Rev. B **61**, 12181 (2000).
[16] B. M. Bartlett and D. G. Nocera, J. Am. Chem. Soc. **127**, 8985 (2005).
[17] K. Matan, D. Grohol, D. G. Nocera, T. Yildirim, A. B. Harris, S. H. Lee, S. E. Nagler, and Y. S. Lee, Phys. Rev. Lett. **96**, 247201 (2006).
[18] I. Dzyaloshinsky, J. Phys. Chem. Solids **4**, 241 (1958).
[19] T. Moriya, Phys. Rev. **120**, 91 (1960).
[20] T. Moriya, Phys. Rev. Lett. **4**, 228 (1960).
[21] A. S. Wills, Phys. Rev. B **63**, 064430 (2001).
[22] M. R. Norman, Rev. Mod. Phys. **88**, 041002 (2016).
[23] M. Elhajal, B. Canals, and C. Lacroix Phys. Rev. B **66**, 014422 (2002).
[24] O. Cépas, C. M. Fong, P. W. Leung, and C. Lhuillier, Phys. Rev. B **78**, 140405(R) (2008).
[25] A. L. Chernyshev and M. E. Zhitomirsky, Phys. Rev. B **92**, 144415 (2015).
[26] L. Messio, S. Bieri, C. Lhuillier, and B. Bernu, Phys. Rev. Lett. **118**, 267201 (2017).
[27] F. A. Gomez Albarracín and P. Pujol, Phys. Rev. B **97**, 104419 (2018).
[28] R. Seshadri and D. Sen, Phys. Rev. B **97**, 134411 (2018).
[29] K. Essafi, O. Benton, and L. D. C. Jaubert, Nat. Commun. **7**, 10297 (2016).
[30] K. Essafi, O. Benton, and L. D. C. Jaubert, Phys. Rev. B **96**, 205126 (2017).
[31] L. Zhang, Y. Wang, J. Lv, and Y. Ma, Nat. Rev. Mater. **2**, 17005 (2017).
[32] H.-K. Mao, X.-J. Chen, Y. Ding, B. Li, and L. Wang, Rev. Mod. Phys. **90**, 015007 (2018).
[33] R. A. Klein, A. B. Altman, R. J. Saballos, J. P. S. Walsh, A. D. Tamerius, Y. Meng, D. Puggioni, S. D. Jacobsen, J. M. Rondinelli, and D. E. Freedman, Phys. Rev. Mater. **3**, 064411 (2019).
[34] J. P. S. Walsh and D. E. Freedman, Acc. Chem. Res. **51**, 1315 (2018).
[35] W. Grochala, R. Hoffmann, J. Feng, and N. W. Ashcroft, Angew. Chem., Int. Ed. Engl. **46**, 3620 (2007).
[36] D. Bloch, J. Phys. Chem. Solids **27**, 881 (1966).
[37] L. S. I. Veiga, M. Etter, K. Glazyrin, F. Sun, C. A. Escanhoela, Jr., G. Fabbris, J. R. L. Mardegan, P. S. Malavi, Y. Deng, P. P. Stavropoulos *et al.*, Phys. Rev. B **96**, 140402(R) (2017).
[38] J. Wang, Y. Feng, R. Jaramillo, J. van Wezel, P. C. Canfield, and T. F. Rosenbaum, Phys. Rev. B **86**, 014422 (2012).
[39] S.-T. Pi, S. Y. Savrasov, and W. E. Pickett, Phys. Rev. Lett. **122**, 057201 (2019).
[40] W. Bi, J. Lim, G. Fabbris, J. Zhao, D. Haskel, E. E. Alp, M. Y. Hu, P. Chow, Y. Xiao, W. Xu, and J. S. Schilling, Phys. Rev. B **93**, 184424 (2016).
[41] D. Haskel, G. Fabbris, J. H. Kim, L. S. I. Veiga, J. R. L. Mardegan, C. A. Escanhoela, Jr., S. Chikara, V. Struzhkin, T. Senthil, and B. J. Kim, Phys. Rev. Lett. **124**, 067201 (2020).
[42] R. A. Klein, J. P. S. Walsh, S. M. Clarke, Y. Guo, W. Bi, G. Fabbris, Y. Meng, D. Haskel, E. E. Alp, R. P. Van Duyne *et al.*, J. Am. Chem. Soc. **140**, 12001 (2018).
[43] These data extend the variable pressure PXRD data known for jarosite. Two previous studies report equation of state information for this mineral. The first extends up to 8.1 GPa: H. Xu, Y. Zhao, J. Zhang, Y. Wang, D. D. Hickmott, L. L. Daemen, M. A. Hartl, and L. Wang, Am. Mineral. **95**, 19 (2010). The second extends the equation of state of jarosite up to 36.2 GPa in R. A. Klein *et al.* [42].
[44] G. S. Pawley, J. Appl. Crystallogr. **14**, 357 (1981).
[45] A. Le Bail, Powder Diffr. **20**, 316 (2005).
[46] See Supplemental Material at http://link.aps.org/supplemental/10.1103/PhysRevLett.125.077202 for full experimental details; additional data, figures, and plots; and details regarding the DFT calculations, which includes Refs. [47–70].
[47] R. Hrubiak, S. Sinogeikin, E. Rod, and G. Shen, Rev. Sci. Instrum. **86**, 072202 (2015).
[48] M. Rivers, V. B. Prakapenka, A. Kubo, C. Pullins, C. M. Holl, and S. D. Jacobsen, High Press. Res. **28** (3), 273 (2008).
[49] D. L. Decker, J. Appl. Phys. **42**, 3239 (1971).
[50] J. P. Walsh, S. M. Clarke, Y. Meng, S. D. Jacobsen, and D. E. Freedman, ACS Cent. Sci. **2**, 867 (2016).
[51] A. Dewaele, M. Torrent, P. Loubeyre, and M. Mezouar, Phys. Rev. B **78**, 104102 (2008).
[52] N. Holmes, J. Moriarty, G. Gathers, and W. Nellis, J. Appl. Phys. **66**, 2962 (1989).

[53] R. Hemley, C. S. Zha, A. P. Jephcoat, H. K. Mao, L. W. Finger, and D. E. Cox, Phys. Rev. B **39**, 11820 (1989).
[54] Y. Akahama and H. Kawamura, J. Appl. Phys. **100**, 043516 (2006).
[55] C. Prescher and V. B. Prakapenka, High Press. Res. **35**, 223 (2015).
[56] A. A. Coelho, *TOPAS Academic: General Profile and Structure Analysis Software for Powder Diffraction Data*, (Bruker AXS, Karlsruhe, Germany, 2007).
[57] R. J. Angel, M. Alvaro, and J. Gonzalez-Platas, Z. Kristallogr. Cryst. Mater. **229** (5), 405 (2014).
[58] U. Bergmann, S. D. Shastri, D. P. Siddons, B. W. Batterman, and J. B. Hastings, Phys. Rev. B **50**, 5957 (1994).
[59] J. P. Perdew, A. Ruzsinszky, G. I. Csonka, O. A. Vydrov, G. E. Scuseria, L. A. Constantin, X. Zhou, and K. Burke, Phys. Rev. Lett. **100**, 136406 (2008).
[60] S. L. Dudarev, G. A. Botton, S. Y. Savrasov, C. J. Humphreys, and A. P. Sutton, Phys. Rev. B **57**, 1505 (1998).
[61] G. Kresse and J. Furthmüller, Comput. Mater. Sci. **6**, 15 (1996).
[62] P. E. Blöchl, O. Jepsen, and O. K. Andersen, Phys. Rev. B **49**, 16223 (1994).
[63] A. Togo and I. Tanaka, Scr. Mater. **108**, 1 (2015).
[64] B. H. Toby, Powder Diffr. **21**, 67 (2006).
[65] A. Sano-Furukawa, H. Kagi, T. Nagai, S. Nakano, S. Fukura, D. Ushijima, R. Iizuka, E. Ohtani, and T. Yagi, Am. Mineral. **94**, 1255 (2009).
[66] M. Benoit, D. Marx, and M. Parrinelo, Nature (London) **392**, 258 (1998).
[67] P. Loubeyre, R. LeToullec, E. Wolanin, M. Hanfland, and D. Hausermann, Nature (London) **397**, 503 (1999).
[68] M. Benoit, A. H. Romero, and D. Marx, Phys. Rev. Lett. **89**, 145501 (2002).
[69] E. Libowitzky, Montash. Chem. **130**, 1047 (1999).
[70] S. D. Jacobsen, J. R. Smyth, R. J. Swope, and R. I. Sheldon, Am. Mineral. **85**, 745 (2000).
[71] F. Birch, Phys. Rev. **71**, 809 (1947).
[72] F. Murnaghan, Proc. Natl. Acad. Sci. U.S.A. **30**, 244 (1944).
[73] H. Ishikawa, T. Okubo, Y. Okamoto, and Z. Hiroi, J. Phys. Soc. Jpn. **83**, 043703 (2014).
[74] D. A. Powers, G. R. Rossman, H. J. Schugar, and H. B. Gray, J. Solid State Chem. **13**, 1 (1975).
[75] K. Sasaki, O. Tanaike, and H. Konno, Can. Mineral. **36**, 1225 (1998), https://rruff-2.geo.arizona.edu/uploads/CM36_1225.pdf.
[76] J. L. Bishop and E. Murad, Am. Mineral. **90**, 1100 (2005).
[77] G. Vankó, J.-P. Rueff, A. Mattila, Z. Németh, and A. Shukla, Phys. Rev. B **73**, 024424 (2006).
[78] Y.-Y. Chang, S. D. Jacobsen, J.-F. Lin, C. R. Bina, S.-M. Thomas, J. Wu, G. Shen, Y. Xiao, P. Chow, D. J. Frost *et al.*, Earth Planet. Sci. Lett. **382**, 1 (2013).
[79] N. Lee, T. Petrenko, U. Bergmann, F. Neese, and S. DeBeer, J. Am. Chem. Soc. **132**, 9715 (2010).
[80] This constraint was used in our DFT simulations to select a reasonable value for the Hubbard U interaction.
[81] C. J. Pollock, M. U. Delgado-Jaime, M. Atanasov, F. Neese, and S. DeBeer, J. Am. Chem. Soc. **136**, 9453 (2014).
[82] Z. Mao, J.-F. Lin, J. Liu, and V. B. Prakapenka, Geophys. Res. Lett. **38**, L23308 (2011).
[83] E. E. Alp, T. M. Mooney, T. S. Toellner, and W. Sturhahn, Hyperfine Interact. **90**, 323 (1994).
[84] W. Sturhahn, E. E. Alp, T. S. Toellner, P. Hession, M. Hu, and J. Sutter, Hyperfine Interact. **113**, 47 (1998).
[85] W. Sturhahn, J. Phys. Condens. Matter **16**, S497 (2004).
[86] P. Materne, W. Bi, E. E. Alp, J. Zhao, M. Y. Hu, A. Jesche, C. Geibel, R. Kappenberger, S. Aswartham, S. Wurmehl *et al.*, Phys. Rev. B **98**, 014517 (2018).
[87] R. Rüffer and A. I. Chumakov, Hyperfine Interact. **97**, 589 (1996).
[88] G. V. Smirnov, U. van Bürck, A. I. Chumakov, A. Q. R. Baron, and R. Rüffer, Phys. Rev. B **55**, 5811 (1997).
[89] W. Sturhahn, Hyperfine Interact. **125**, 149 (2000).
[90] S. Klotz, J. Chervin, P. Munsch, and G. Le Marchand, J. Phys. D **42**, 075413 (2009).
[91] W. M. Xu, G. R. Hearne, S. Layek, D. Levy, J.-P. Itié, M. P. Pasternak, G. Kh. Rozenberg, and E. Greenberg, Phys. Rev. B **95**, 045110 (2017).
[92] T. C. Gibb, *Principles of Mössbauer Spectroscopy* (Springer, Norwich, 2013).
[93] D. P. Dickson and F. J. Berry, *Mössbauer Spectroscopy* (Cambridge University Press, Cambridge, England, 2005).
[94] S. Hayashida, H. Ishikawa, Y. Okamoto, T. Okubo, Z. Hiroi, M. Avdeev, P. Manuel, M. Hagihala, M. Soda, and T. Masuda, Phys. Rev. B **97**, 054411 (2018).
[95] M. A. de Vries, T. K. Johal, A. Mirone, J. S. Claydon, G. J. Nilsen, H. M. Rønnow, G. van der Laan, and A. Harrison, Phys. Rev. B **79**, 045102 (2009).
[96] P. Bonville, V. Dupuis, E. Vincent, P. E. Lippens, and A. S. Wills, in *ICAME 2005* (Springer, Dordrecht, 2006), pp. 1085–1089.
[97] K. Matan, T. Ono, Y. Fukumoto, T. J. Sato, J. Yamaura, M. Yano, K. Morita, and H. Tanaka, Nat. Phys. **6**, 865 (2010).
[98] M. R. Norman, N. J. Laurita, and D. Hsieh, Phys. Rev. Research **2**, 013055 (2020).
[99] R. P. Dias and I. F. Silvera, Science **355**, 715 (2017).
[100] H. Luo, S. Desgreniers, Y. K. Vohra, and A. L. Ruoff, Phys. Rev. Lett. **67**, 2998 (1991).
[101] M. P. Pasternak, R. D. Taylor, A. Chen, C. Meade, L. M. Falicov, A. Giesekus, R. Jeanloz, and P. Y. Yu, Phys. Rev. Lett. **65**, 790 (1990).
[102] M. P. Pasternak, W. M. Xu, G. Kh. Rozenberg, R. D. Taylor, G. R. Hearne, and E. Sterer, Phys. Rev. B **65**, 035106 (2001).
[103] W. M. Xu and M. P. Pasternak, Hyperfine Interact. **144**, 175 (2002).

Correction: A proof request to insert additional "Corresponding author" byline footnotes was overlooked and has been rectified.